

Predicting spin orbit coupling effect in the electronic and magnetic properties of cobalt (Co) doped WSe₂ monolayer

Dinesh Thapa

*Department of Physics & Astronomy and Center for Computational Sciences,
Mississippi State University, Mississippi State, MS, 39762, USA and
Department of Chemistry and Biochemistry, North Dakota State University, Fargo, ND, 58108, USA*

Dinh Loc Duong, Seok Joon Yun, and Young Hee Lee

*Center for Integrated Nanostructure Physics (CINAP), Institute for Basic Science (IBS),
Sungkyunkwan University (SKKU), Suwon 16419, Republic of Korea and
Department of Energy Science, Sungkyunkwan University (SKKU), Suwon 16419, Republic of Korea*

Santosh KC

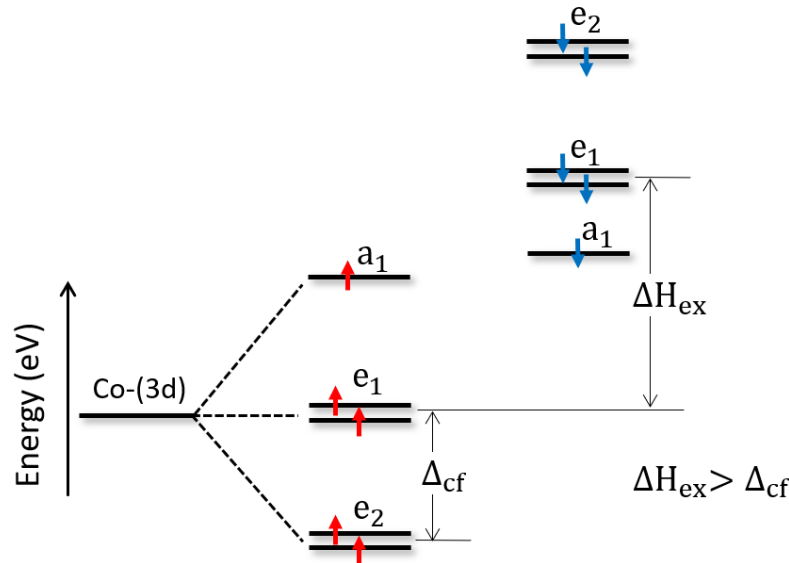
Chemical and Materials Engineering, San Jose State University, San Jose, California 95112, USA

Seong-Gon Kim*

*Department of Physics & Astronomy and Center for Computational Sciences,
Mississippi State University, Mississippi State, MS, 39762, USA*

(Dated: October 2021)

The electronic and magnetic properties of cobalt (Co) doped monolayer (ML) tungsten diselenide (WSe₂) are investigated using the density functional theory with the on-site Hubbard potential correction (DFT+U) for the localized *d* orbitals of Co atom taking into account the spin orbit coupling (SOC) interaction. The results show that the substitution of Co at the W sites of ML WSe₂ is energetically favorable under Se rich environment. We noticed that the Hund's exchange splitting (ΔH_{ex}) is dominant over the crystal field splitting (Δ_{cf}). The induced magnetic moment due to the Co-doped defect is $\sim 3.00 \mu_B$ per Co atom. The magnetic interaction between two Co atoms at the nearest neighbor separation depends mainly on the concentration of the impurity atoms. The calculated value of curie temperature (T_C) is increasing with increasing impurity concentration satisfying the Zener model. Based on the results, it can be proposed that the Co-doped WSe₂ monolayer is potential candidate to apply in spintronics, optoelectronics, and magnetic storage devices.



* Corresponding author: sk162@msstate.edu

I. INTRODUCTION

The discovery of graphene as a promising 2D material in 2004 [1], has led to an extensive search of other possible 2D materials. The transition metal dichalcogenide (TMDCs) with stoichiometric formula MX_2 ($\text{M} = \text{Mo}, \text{W}$; $\text{X} = \text{S}, \text{Se}, \text{Te}$) have become an appealing 2D materials because of their fascinating properties like layer dependent narrow band gap ranging from visible to near infra-red [2, 3], strong spin (Zeeman) splitting [4, 5], strain resistant [6, 7], long-lived valley polarization [8], odd-parity superconductivity [9], gate-controlled magneto-resistance [10], and large absorption coefficient [11]. TMDCs are proven to have a widespread applications in electrical devices like the thin film solar cells [12], single-layer transistors [13], hydrogen storage [14], ultra-sensitive chemical sensors, Li-ion batteries [15], flexible and wearable electronic devices [7], etc. The intrinsic physical, chemical, mechanical, and optical properties of TMDCs monolayer (ML) can be further tuned by the introduction of impurity atoms by means of doping and adsorption, and by the structural defect mechanism such as creating vacancy on the lattice sites which considerably enlarges their applications in electronics, photonics, and spintronics. Notably, the spin polarization induced in nonmagnetic TMDC materials by doping magnetic TM atoms surprisingly changes electrical resistivity with temperature due to scattering of conduction electrons. This phenomenon which is commonly observed in nanomaterial electronics is called Kondo effect [16]. Depending upon the type of polymorphs, and the number of interacting valence electrons of the doped element, ML-TMDCs may behave as a metallic, half-metallic, semiconductors, topological insulators, and superconductors [9, 17–19]. In case of TM-doped TMDCs monolayer, there exists a strong orbital interaction between impurity atoms with that of host metal and chalcogen atom that gives them unique electronic and magnetic properties.

In the present paper, We have tailored the electronic and magnetic properties of 2D ML- WSe_2 via the substitutional doping of TM cobalt (Co) atom with the inclusion of spin orbit coupling (SOC) which eventually leads to dilute magnetic semiconductor (DMS). DMSs are the materials which possess the combined semiconducting and magnetic properties within the same material. These materials exhibits promising applications for new generation magneto-optics, and 2D spintronic devices such as spin based FETs, magnetic bipolar transistors (MBTs), filters, diodes, spin qubits in quantum computers, and magneto-resistive memories, etc [20–23]. The DMSs materials based on spin electronics are far better than other traditional devices both in terms of mechanical efficiency and energy consumption. It has been known from numerous theoretical and experimental studies that the most of the transition metal doped 2D materials are found to exist as DMS materials with carrier mediated ferromagnetism (FM) which find their tremendous applications mainly in nanoscale spintronics. Meanwhile, spintronics is the phenomenon of producing and storing electronic transport information based on the charge and spin of the electrons which is practically more relevant for novel electronic devices [24]. Xu Zhao et al. predicted theoretically that Ni, Pd and Pt doped WS_2 as a potential candidates for the thin DMSs [25]. Bo Li et al. created experimentally the ferromagnetic 2D DMSs materials by doping Fe in ML SnS_2 exfoliated using a micromechanical cleavage method [26]. S. M. Hailemariam suggested that Mn-doped bilayer MoS_2 are promising candidates for 2D DMS for high-temperature spintronics applications [27]. Y. C. Cheng et al. demonstrated that 2D DMS can be realized by doping ML MoS_2 by Mn, Fe, Co, and Zn [20]. Weiyang Yu et al. found that the TM (Ti, V, Cr, Mn, Fe, and Ni) doped black phosphorenes show the DMS properties [28]. Since, WSe_2 exhibits the most robust excitonic valley polarization among other TMDCs owing to the large spin orbit splitting [29], the Co doped WSe_2 is supposed to exhibit its importance in valleytronics besides spintronics and optoelectronics. Moreover, the ferromagnetic (FM) ordering is required for the 2D nanoscale magnets to be used in nanoelectronics and this property is found to be inherent in Co doped WSe_2 monolayer. Also, we estimated the Curie temperature (T_C) using the mean-field approximation (MFA) for the ferromagnetic (FM) cases. Surprisingly, the typically high value of magnetic anisotropy energy (MAE) has been observed with such defect in WSe_2 monolayer which opens the possible gate for their applications in magnetic storage devices [30].

II. COMPUTATIONAL METHODS

In this paper, we presented the detailed description of structural, electronic, and magnetic properties of Co doped on the monolayer of Tungsten diselenide (WSe_2) using GGA+U. The density functional theory (DFT) calculations were performed using the projector augmented wave (PAW) method to describe the ionic cores [31] and the plane wave basis set method as implemented within the Vienna ab initio simulation package (VASP) [32, 33]. We used the Perdew-Burke-Ernzerhof (PBE) functional to describe the exchange-correlation interactions as in our previous calculations [34–36]. On account of the strongly correlated electronic systems, we employed the GGA+U method within Dudarev’s approach [37] for the on-site Coulomb interaction in the localized d orbitals of Co atom. In the present work, a corrected U value for Co atom, which best describes the electronic and magnetic properties of the system, was selected. The correction parameter of effective $U_{\text{eff}} = U - J = 3.3$ eV was chosen throughout the calculations with $J = 1.0$ eV as previously determined by Wang et al. [38] where the correction parameter U has been determined by fitting the calculated and experimental formation enthalpies of metal oxides. It has been found from several

theoretical studies that the value $U_{\text{eff}}=3.3$ eV for Co lies typically within the acceptable range to describe the various ground state energies, electrochemical, and magnetic properties of the cobalt based system [39–44]. The effective U values for all other atoms W, and Se were set zero. We did the convergence test for cut off energy and vacuum length separately for $5 \times 5 \times 1$ supercell doped with single Co atom. From the convergence test, we found that the kinetic energy cut off for the plane wave expansion was sufficient to set up at 425 eV and minimum vacuum length of 18 Å was added perpendicular to the monolayer of WSe₂ to safely avoid spurious interaction between neighboring layers. The Brillouin zone integration was sampled using gamma centered k-mesh of $6 \times 6 \times 1$, $4 \times 4 \times 1$, and $2 \times 2 \times 1$ for the structural relaxations in $5 \times 5 \times 1$, $7 \times 7 \times 1$, and $10 \times 10 \times 1$ supercells using tetrahedron method of Blöchl correction [45] with smearing width of 0.01 eV in all the calculations except for the $10 \times 10 \times 1$ supercell where the electron occupation were smeared with Gaussian distribution function. All the structures were fully relaxed including cell parameters and atom positions until the energy value reaches the precision of 10^{-5} eV and the residual force less than 0.02 eV/atom except for the supercells of $5 \times 10 \times 1$, $6 \times 12 \times 1$, $7 \times 14 \times 1$, and $8 \times 16 \times 1$ in which the residual force was less than 0.04 eV/atom owing to the large size of the supercells. All the calculations were spin polarized taking into account the spin orbit coupling (SOC) effect with non-collinear calculations in VASP interface, and the magnetic moments were initialized parallel to the c -axis. The relaxed geometry from the standard collinear calculations were used to obtain full relativistic energy values in all the non-collinear calculations switching off the symmetry. The geometrical structures, and spin densities were visualized using VESTA code [46]. All the band structure plots were produced using the program PYPROCAR [47].

III. RESULTS AND DISCUSSION

We carried out the first principle investigations to perform a single point doping of Co atom on the W atom for three different sizes $5 \times 5 \times 1$ (75 atoms), $7 \times 7 \times 1$ (147 atoms), and $10 \times 10 \times 1$ (300 atoms) of the supercell structures which corresponds to 4.0 %, 2.0 %, and as low as 1.0 % atomic concentration of Co in order to match with that of experiment [48] where the relaxed Co-Co distance is at 16.61 Å, 23.23 Å, and 33.18 Å respectively. The respective pseudopotential valence electron configurations for W, Se, and Co are $5d^46s^2$, $4s^24p^4$, and $3d^74s^2$. To check the accuracy of our calculations we first calculated the relaxed structural lattice parameter, and the electronic band structure for the primitive unit cell structure of WSe₂ monolayer (ML). Our calculated lattice parameter was $a=b=3.32$ Å which agrees well with the experimental value of 3.29 Å [49] and previously reported calculated values [50]. The optimized lattice parameter for monolayer was used to replicate the lattice parameter for the bigger unit cells. Since, the standard GGA underestimates the band gap value, our calculated value of band gap for primitive WSe₂ monolayer without using SOC is 1.55 eV and that using SOC is 1.26 eV that underestimates the experimentally reported value of 1.65 eV; however, it is consistent with the others computed values. The band gap value for the pristine ML of $7 \times 7 \times 1$ supercell also agrees with that of primitive ML both in non-SOC and SOC. We further illustrated that the band structure of the supercell ML is unfolded accurately into the band structure of primitive ML. All of these confirm that monolayer and super cell structures we used for our calculations are valid. The band structure plots for monolayer of primitive and $7 \times 7 \times 1$ supercell of pristine WSe₂ without and with using SOC are shown in Fig.1 and Fig.5. Also, the unfolded band structure for the pristine $7 \times 7 \times 1$ supercell into the band structure of primitive ML in non-SOC case is produced using the BANDUP code [51, 52] and is displayed in Fig.3.

The WSe₂ monolayer belongs to the space group of $p\bar{6}m2$ (D_{3h}^1) in which W atom is sandwiched between two Se atoms and exhibits trigonal prismatic coordination with Se atoms. The stacking Se-W-Se is coupled together with strong covalent bonding while the inter-layer distance is separated by weak van der Waal (vdW) force. Since, the pristine WSe₂ monolayer is non-magnetic; hence, we theoretically aimed to induce the magnetic properties in WSe₂ monolayer via the substitutional doping of TM-Co on W atom. Our numerical calculations show that the Co-Se bond length is 2.56 Å after the geometrical relaxation which is slightly more than that of the W-Se bond length of 2.54 Å in pristine WSe₂ layer. The surrounding W-Se bond length in the vicinity of doped atom is 2.55 Å. The W-Se bond length far away from doping site is unchanged. The Co-Se-W bond angle in the Co-defect WSe₂ is 82.78° and the W-Se-W bond angle in pristine and in the defect WSe₂ are 81.31° and 81.31° respectively. Similarly, the nearest Se-Se bond length for the two Se atoms one on each sub layer denoted by (Se – Se₁) and on the same sub-layer denoted by (Se – Se₂) for the pristine and defect cases are annotated in the Fig.4. Also, the optimized lattice parameter in case of doped supercell is found to be increased by 1.80 % than that of pristine supercell.

Here, the defect due to the substitution of Co atom on the host W atom is represented by Co_W. The formation energy $\Delta E(\text{Co}_W)$ of the defect is defined as,

$$\Delta E(\text{Co}_W) = E_{\text{Doped}} - E_{\text{Pristine}} - n\mu_{\text{Co}} + n\mu_{\text{W}} \quad (1)$$

where, E_{Doped} , and E_{Pristine} are the relaxed total energies of the supercell of the doped and pristine ML-WSe₂ respectively. μ_{Co} , and μ_{W} are the chemical potential of the single stable atom of hexagonal Co ($P6_3/mmc[n^\circ 194]$), and bcc W ($Im\bar{3}m[n^\circ 229]$). n is the number of W atoms replaced by Co dopants. μ_{W} is defined within a range of

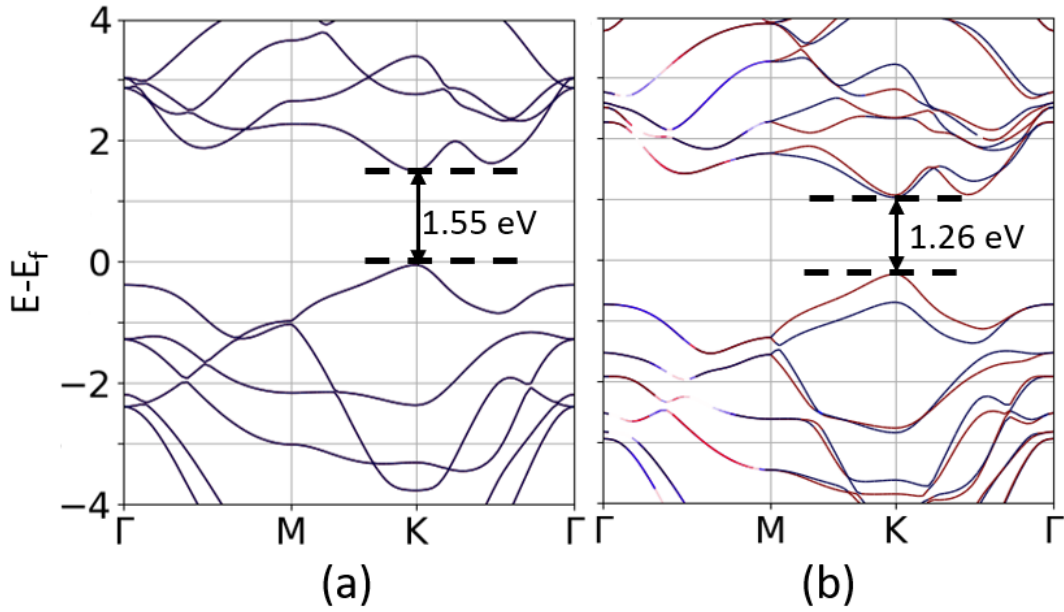


FIG. 1: Band structures of primitive monolayer of pristine WSe₂ with (a) non-SOC, and (b) SOC showing blue (spin down) and red (spin up) bands. Fig.(a) shows the bands are degenerate without the inclusion of SOC while in Fig.(b) the bands undergo spin split at high symmetry kpoint K due to SOC effect. The zero of the energy axis represents the Fermi level.

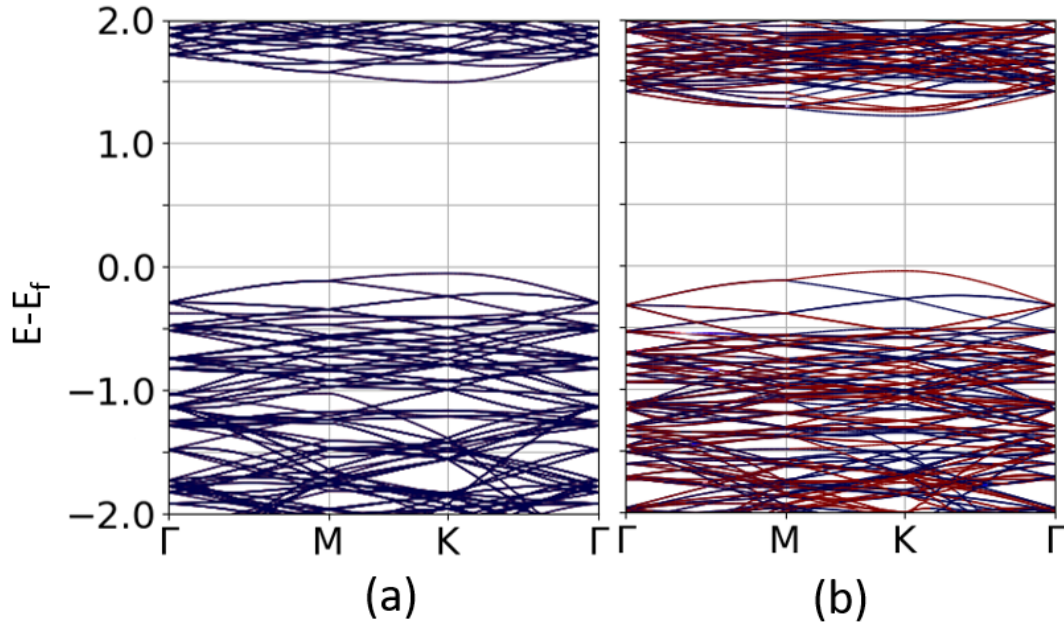


FIG. 2: Band structures of pristine monolayer of $7 \times 7 \times 1$ WSe₂ supercell with (a) non-SOC, and (b) SOC showing blue (spin down) and red (spin up) bands. The zero of the energy axis represents the Fermi level.

values corresponding to W-rich or Se-rich growth environment. At W-rich limit, μ_W is equal to the total energy per W atom in its *bcc* bulk phase. At Se-rich limit μ_{Se} is the total energy of single atom in the bulk reference phase of monoclinic Se ($P2_1/c[n^\circ 14]$) in which

$$\mu_W = \mu_{WSe_2} - 2\mu_{Se} \quad (2)$$

where, μ_{WSe_2} is equal to the total energy per formula unit of the pristine ML of WSe₂ [53]. Without the inclusion of

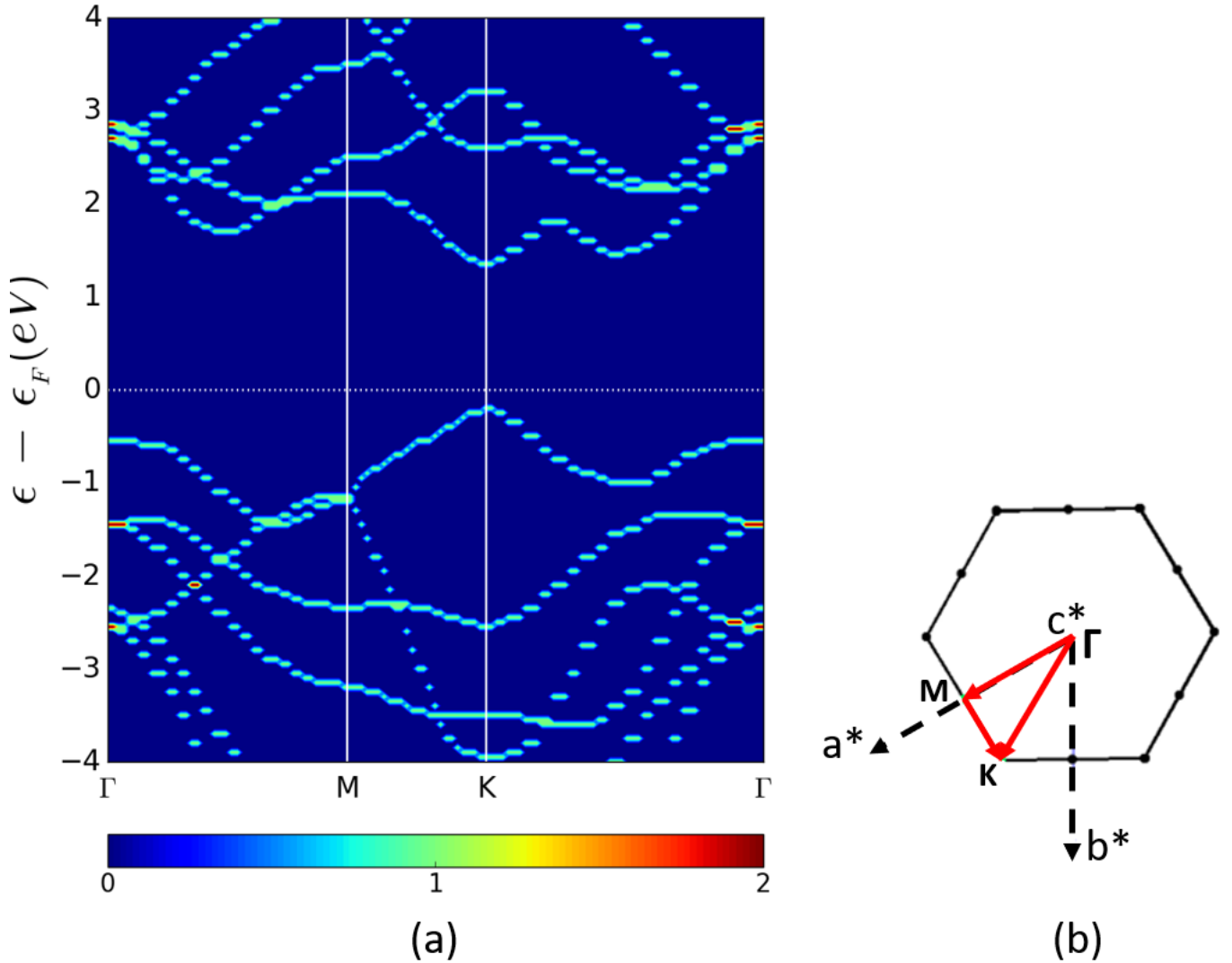


FIG. 3: (a) Unfolded band structure of pristine monolayer of $7 \times 7 \times 1$ WSe₂ supercell into primitive monolayer with non-SOC. The color scale in the bottom shows the number of bands in the primitive cell crossing the energy interval at a given primitive wave vector. (b) First Brillouin zone diagram of primitive ML of WSe₂ represented by solid red line showing high symmetry kpoints, $\Gamma(0,0,0)$, $M(1/2,0,0)$, and $K(1/3,1/3,0)$.

SOC, we found that the formation energy for the Co-doped WSe₂ monolayer is 3.00 eV and 1.37 eV, and with the inclusion of SOC these values are 2.82 eV and 1.24 eV under W-rich and Se-rich growth conditions respectively which means that Co_W defect is energetically favourable at Se-rich condition. Recently, S. Ahmed et al. experimentally studied the magnetic properties of Co doped WSe₂ monolayer by implantation. Their reports on XRD and Raman analysis indicated that Co successfully substitutes on W site in which Co exists as Co⁺² state [48]. Our calculated value of formation energy without SOC for Co_W defect corroborates the result obtained by Ninghua Wu et al. [54].

Further, we studied the changes in electronic and magnetic properties within the host WSe₂ due to the impurity doping. Since the Co atom has 3 additional valence electrons compared to W atom which is responsible to create significant electronic and magnetic changes in the doped system. Fig.5 depicts the spin polarized total band structures for ML of supercells $5 \times 5 \times 1$, $7 \times 7 \times 1$, and $10 \times 10 \times 1$, taking into account the non-SOC and SOC effect. Further, the *d*-bands of the impurity atom are localized within the bandgap of the host WSe₂ monolayer. In order to shed light on the electronic properties of Co-doped WSe₂ monolayer, we calculated the orbital projected band structures as represented in Fig.6 and 7 respectively for ML of $7 \times 7 \times 1$ supercell. At both the conditions, the impurity levels near to the Fermi level are mainly contributed by the 3*d* state of the dopant, 5*d* state of the nearest W atoms, and 4*p* state of the Se atoms where W-5*d* (*d*_{z²}, and *d*_{*x*²-*y*²}) and Co-3*d* states are strongly localized, and the nearby Se-4*p* is delocalized. We found partial contribution from W-*d*_{*x**y*} and no any contribution from W (*d*_{*x**z*}, and *d*_{*y**z*}) near the

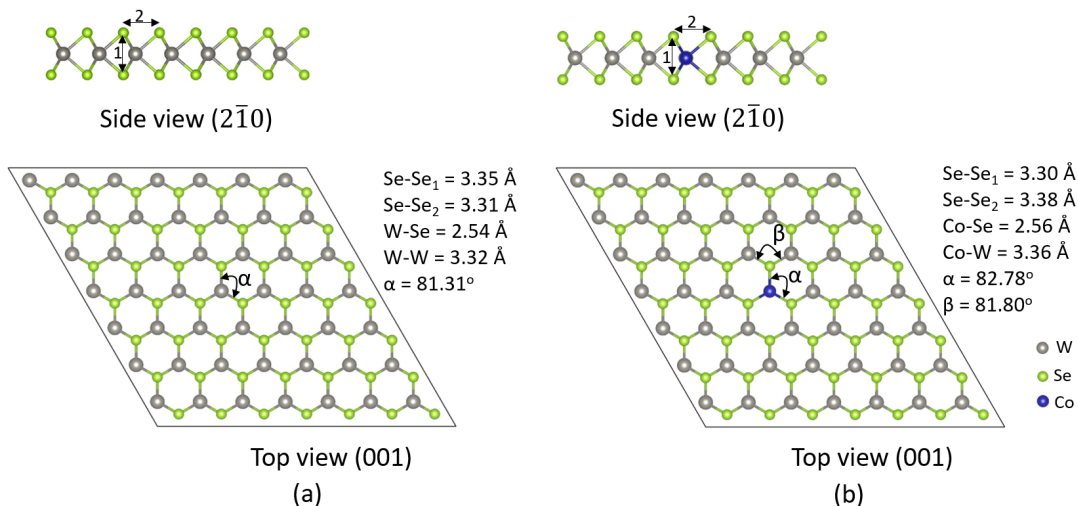


FIG. 4: Relaxed geometrical structures of (a) pristine and (b) Co_W defect WSe_2 monolayer in $7 \times 7 \times 1$ supercell.

Fermi level. Due to the trigonal coordination of the W and Se atoms, the $3d$ state of Co-atom split into three groups namely i) a doubly degenerate occupied bonding state e_2 (d_{yz} , d_{xz}), ii) singly degenerate unoccupied anti-bonding state a_1 (d_{z^2}), and iii) doubly degenerate partially occupied state e_1 (d_{xy} , and $d_{x^2-y^2}$). Consequently, there is strong hybridization of W- $5d$ state, Co- e_2 state, and partial hybridization of Co-(a_1 , and e_1) states with Se- $4p$ state. The projected band structure using SOC shows that the unoccupied a_1 lies between the lowest spin down and the highest spin up bands of e_1 state above the Fermi level. Therefore, only the a_1 (d_{z^2}) state is the fully unoccupied d -orbital in Co-doped WSe_2 . The orbitals d_{yz} and d_{xz} from e_2 state overlap with each other and position themselves below the Fermi level. Also, there is overlapping between the orbitals d_{xy} and $d_{x^2-y^2}$ from e_1 state with their spin up bands close to Fermi level and spin down bands furthest away above the Fermi level. In addition, the localization of the W- $3d$ bands near the Fermi level goes on decreasing as the distance from the Co-atom increases. Thus, the orbital hybridization via $p-d$ exchange interaction among dopant Co, W, and Se atoms is giving rise to the magnetic properties in the Co-doped WSe_2 monolayer. This effect of producing magnetic moment on TMDCs by reducing the symmetry via the localization or delocalization of the d -bands of impurity atom is commonly called Jahn-Teller distortion effect [55]. We estimated the approximate crystal field splitting $\Delta_{\text{cf}} = e_1^\uparrow - e_2^\uparrow$ as 0.20 eV in non-SOC and 0.12 eV in SOC. Similarly, the Hund's exchange energy splitting, $\Delta H_{\text{ex}} = e_1^\downarrow - e_1^\uparrow$ is 0.57 eV in non-SOC, and 0.45 eV in SOC. Here, $\Delta H_{\text{ex}} > \Delta_{\text{cf}}$ dictates the dominant nature of Hund's exchange splitting over crystal field splitting due to which e_2^\downarrow has lower energy than a_1^\downarrow and e_1^\downarrow . However, the study performed by B. Huang et al. in Co_B defect which is the cobalt substituted in Boron atom in single-layer boron-nitride (SLBN), the crystal field (Δ_{cf}) splitting is dominant over Hund's exchange splitting (ΔH_{ex}) [56]. The dominating nature of ΔH_{ex} over Δ_{cf} was observed by Carmen J. Gil et al. in Ni doped WSe_2 [57] but the Co doped WSe_2 in their case suggests non-magnetic properties due to the delocalization of the impurity band which is in contrast to our present work where the impurity band is strongly localized near the Fermi level. Our numerical prediction is still valid since Co-doped WSe_2 exhibits strong magnetic properties experimentally with large local magnetic moment on Co-atom which is consistent with our theoretical results. The localization of the d -orbitals in the present work is similar in non-SOC and SOC except that the SOC lifted the degeneracy of the twicely folded bands opening a distinct direct band gap at K-point (for 4.0% Co doping) and at Γ -point (for 2.0 % and 1.0 % Co doping). Our band structure calculation using SOC proves that Co-doped WSe_2 monolayer is a dilute magnetic semiconductor in ground state. On the other hand without the inclusion of SOC, the doped system is behaving as a half-metal with wide band gap in a minority spin channel in all type of dopant concentrations. We further calculated the 3D iso-surface and 2D contour plots of magnetization density to investigate the distribution of the spin polarization due to Co_W defect. We observed the spin polarization is mainly localized on the impurity atom and the nearby W and Se atoms surrounding the interstitial regions between them. The induced magnetic moment due to the defect Co_W is $3.00 \mu_B$ and $2.98 \mu_B$ per Co atom respectively without using SOC and with using SOC. The strong hybridization between Co- $3d$ state and the nearest Se- $4p$ state causes the significant spin splitting to the nearby six Se atoms as well. We can observe the parallel or anti-parallel coupling between impurity Co-atom and W atoms via the nearest Se atoms. In case of 2.0 % and 1.0 % impurity concentrations, the spin polarization of the nearby six Se atoms (Se_{N1}) dictates the ferromagnetic (FM) coupling with the impurity atom (Co) leaving the net spin polarization on the nearest six W-atoms (W_{N1}) zero. Similarly, the second, third, and fourth nearest W-atoms (W_{N2} , W_{N3} , and W_{N4}) undergo AFM, FM, and AFM interaction with Co-atom respectively.

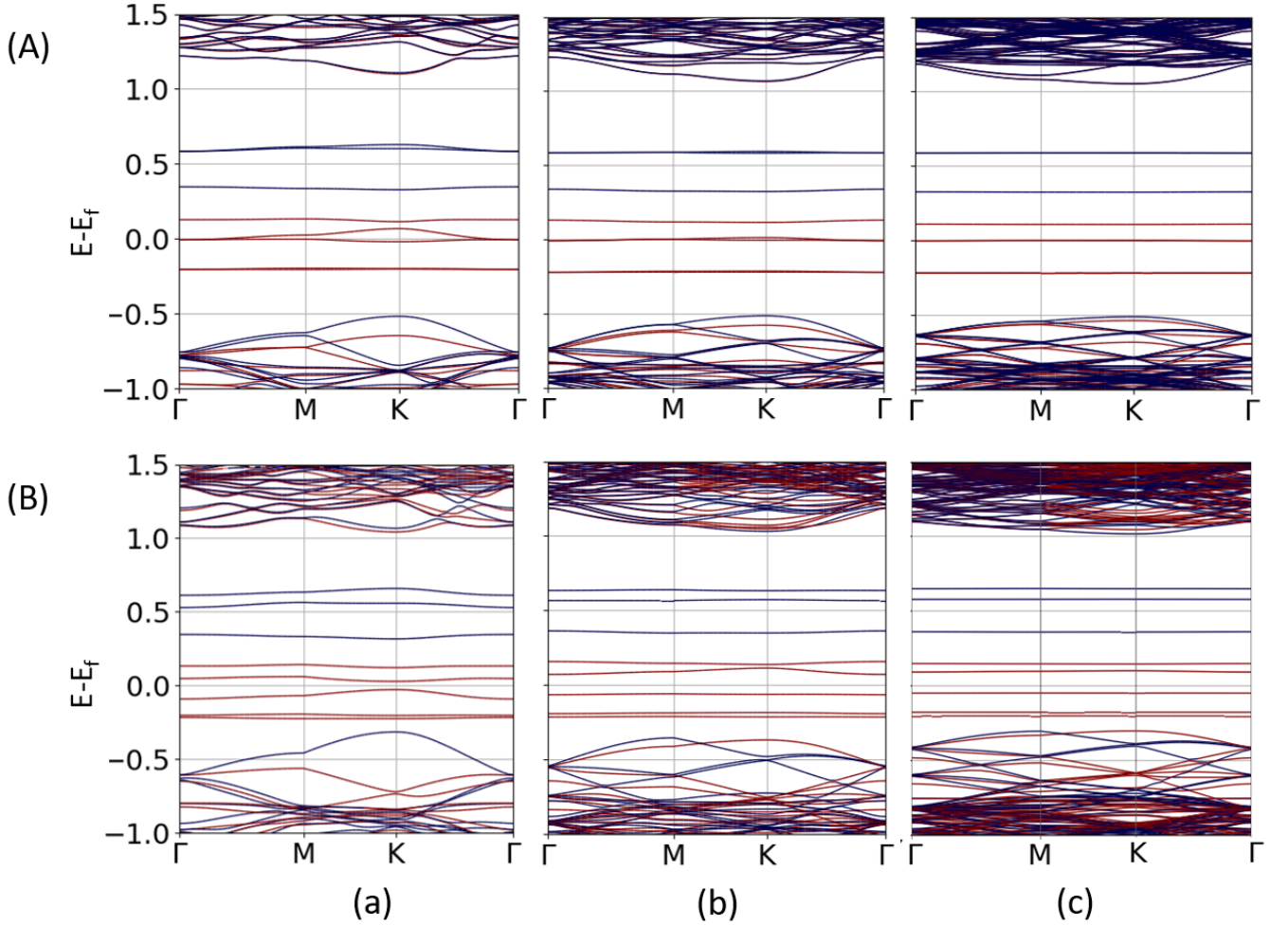


FIG. 5: Total band structures of Co-doped ML-WSe₂ in supercell size of (a) $5 \times 5 \times 1$, (b) $7 \times 7 \times 1$, and (d) $10 \times 10 \times 1$ with (A) non-SOC and (B) SOC. The defect systems are half metallic with wide band gap along spin down channel without SOC: however, it opens a wide band gap when SOC effect is introduced. The zero of the energy axis represents the Fermi level.

Eventually, the W atoms far away from the Co-atom exhibit anti-parallel alignment with impurity atom within the inclusion of SOC effect. We found, the total magnetic moment induced on the system is larger than the local magnetic moment on the Co-atom which is attributed to the parallel spin polarizations of the nearby six Se atoms with the impurity atom Co. Also, the magnetization density map reveals the fact that a significant portion of spin down charges are induced in the interstitial region between six nearest W atoms and Co-atom as shown in Fig.8. The total magnetic moment on the super cells of impurity concentrations 4.0%, 2.0%, and 1.0% with the local magnetic moments induced on the Co-atom, and the first, second, third, and fourth nearest W atoms (W_{N1} , W_{N2} , W_{N3} , W_{N4}) and Se atoms (Se_{N1} , Se_{N2} , Se_{N3} , Se_{N4}) from impurity Co atom are annotated in Table. I (for non-SOC calculations) and Table.II (for SOC calculations) where the average distance of W_{N1} , W_{N2} , W_{N3} , and W_{N4} are found to be 3.35 Å, 5.75 Å, 6.65 Å, and 8.78 Å and that of Se_{N1} , Se_{N2} , Se_{N3} , and Se_{N4} are 2.55 Å, 4.16 Å, 5.36 Å, 7.11 Å respectively from the Co-atom.

The plots on magnetization density using SOC confirms that the spin down channel of delocalized charges is uniformly distributed over the entire W atoms. In the similar study performed by D.L. Duong, et al. with vanadium (V) doped WSe₂ monolayer, the impurity atom V and W atoms have FM coupling over the long range [58]. Here, the magnetic interaction between doped Co, and W atoms in Co_W defect is limited within short range without SOC. Thus, the long range magnetic order in the host material with W as a polarized charge carriers is significantly observed within the inclusion of SOC as shown in Fig.9. Similarly, Fig.10 represents the 3D iso-surface plot of band decomposed charge density of valence band maximum (VBM) and conduction band minimum (CBM) which elucidates that the bands VBM, and CBM across the Fermi level are mainly contributed by the spin up density of the dopant atom Co, nearest W, and Se atoms.

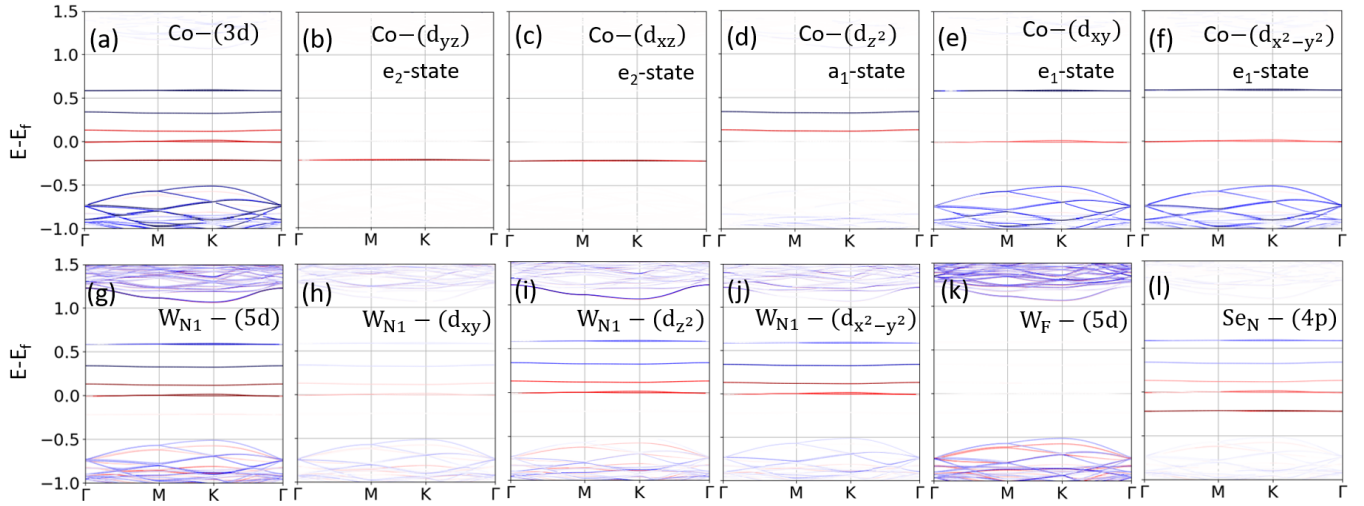


FIG. 6: Orbital projected band structures of $7 \times 7 \times 1$ supercell of Co_W defect with non-SOC. (a) Projected band structure of Co-(3d) state. (b,c) Projected band structures representing Co e_2 states (d_{yz} , and d_{xz}), (d,e) a_1 state (d_{z^2}), and (f) e_1 states (d_{xy} and $d_{x^2-y^2}$), (g) orbital projected band structure of nearest tungsten W_{N1} -(5d) state, (h) W_{N1} - d_{xy} state, (i) W_{N1} - d_{z^2} state (j) W_{N1} - $d_{x^2-y^2}$ state, (k) projected band structure for furthest tungsten W_F -(5d) state, and (l) projected band structure of the nearest selenide Se_N -(4p) state from Co atom.

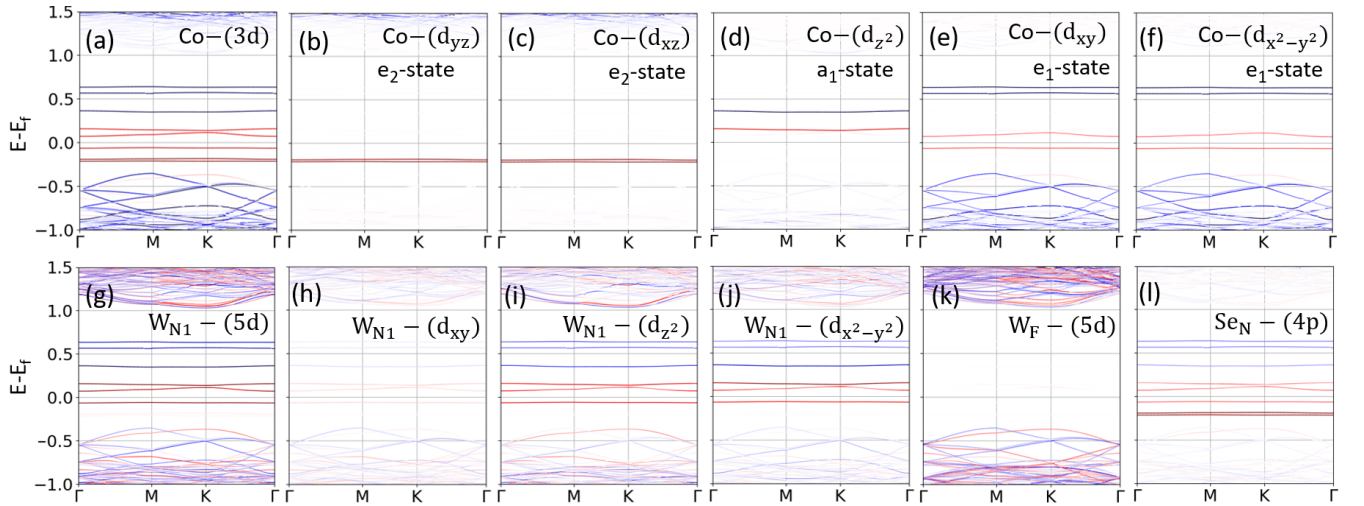


FIG. 7: Orbital projected band structure of $7 \times 7 \times 1$ supercell of Co_W defect with SOC. (a) Projected band structure of Co-(3d) state. (b,c) Projected band structures representing Co e_2 states (d_{yz} , and d_{xz}), (d,e) a_1 state (d_{z^2}), and (f) e_1 states (d_{xy} and $d_{x^2-y^2}$), (g) orbital projected band structure of nearest tungsten W_{N1} -(5d) state, (h) W_{N1} - d_{xy} state, (i) W_{N1} - d_{z^2} state (j) W_{N1} - $d_{x^2-y^2}$ state, (k) projected band structure for the furthest tungsten W_F -(5d) state, and (l) projected band structure of the nearest Selenide Se_N -(4p) state from Co atom.

TABLE I: Calculated total magnetic moment per supercell (m_t), magnetization (M), local magnetic moments induced on Co, and the first, second and third nearest W, and Se atoms (W_{N1} , W_{N2} , W_{N3} , and Se_{N1} , Se_{N2} , Se_{N3}) from the Co-atom, and the half metallic band gap ($E_{g0.5}$) using collinear calculations (non-SOC) for 4.0 %, 2.0 %, and 1.0 % impurity concentrations.

Concentration	m_t (μ_B)	M (emu/g)	Co (μ_B)	W_{N1} (μ_B)	W_{N2} (μ_B)	W_{N3} (μ_B)	W_{N4} (μ_B)	Se_{N1} (μ_B)	Se_{N2} (μ_B)	Se_{N3} (μ_B)	Se_{N4} (μ_B)	$E_{g0.5}$ (eV)
4.0 %	3.00	1.99	2.26	-0.008	-0.001	0.010	-0.001	0.084	-0.003	0.003	0.000	0.84
2.0 %	3.00	1.67	2.26	-0.008	0.001	0.009	-0.001	0.083	-0.003	0.003	0.000	0.84
1.0 %	2.99	0.49	2.26	-0.009	0.001	0.009	-0.001	0.084	-0.003	0.003	0.000	0.84

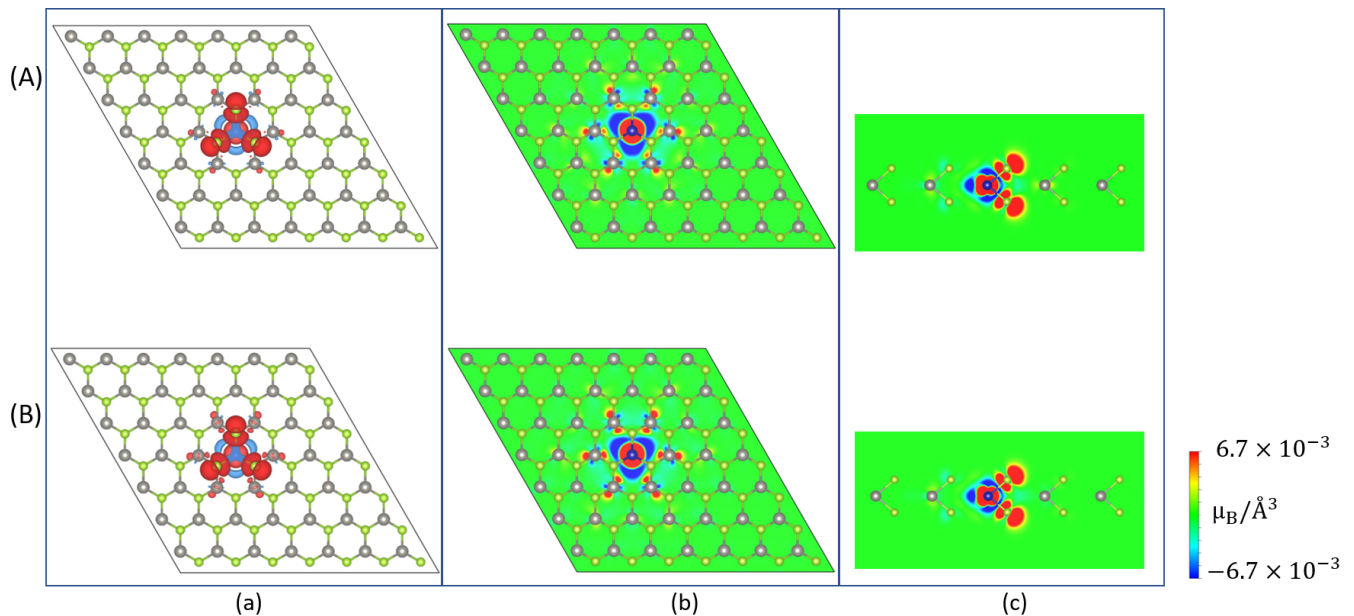


FIG. 8: (a) 3D representation of iso-surface, (b) top view (001), and (c) side view ($2\bar{1}0$) of 2D contour plot of magnetization density in $7 \times 7 \times 1$ supercell (2.0 % impurity concentration) within the range $\pm 6.7 \times 10^{-3} \mu_B/\text{\AA}^3$ for spin down in blue and spin up in red using (A) non-SOC and (B) SOC.

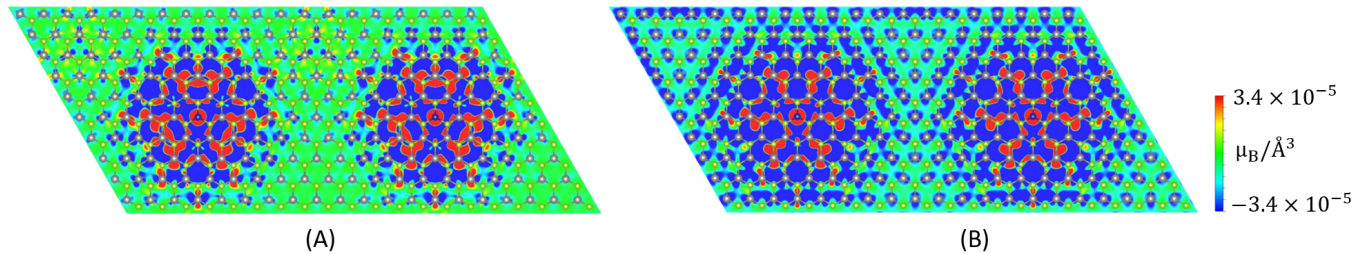


FIG. 9: Top view (001) of 2D contour plot of magnetization density in $10 \times 10 \times 1$ supercell (1.0% impurity concentration) within the range $\pm 3.4 \times 10^{-5} \mu_B/\text{\AA}^3$ for spin down in blue and spin up in red color respectively with (A) non-SOC and (B) SOC.

The magnetic interaction including ferromagnetic (FM), and anti-ferromagnetic (AFM) configurations was studied in two different ways, (a) varying impurity concentration and distance between two dopant atoms simultaneously, (b) varying impurity concentration with two dopant atoms fixed at equilibrium spatial positions. For this purpose, the supercell of different sizes $2 \times 2 \times 1$, $2 \times 4 \times 1$, $3 \times 6 \times 1$, $4 \times 8 \times 1$, $5 \times 10 \times 1$, $6 \times 12 \times 1$, $7 \times 14 \times 1$ and $8 \times 16 \times 1$ were considered with impurity concentration 50.0%, 25.0%, 11.1%, 6.2%, 4.0%, 2.8%, 2.0%, and 1.6% respectively. The spatial position of two Co atoms in these supercells were so chosen that they lie at a furthest distance satisfying

TABLE II: Calculated total magnetic moment per supercell (m_t), magnetization (M), local magnetic moments induced on Co, and first, second and third nearest W, and Se atoms (W_{N1} , W_{N2} , W_{N3} , and Se_{N1} , Se_{N2} , Se_{N3}) from the Co-atom, and the band gap (E_g) using non-collinear calculations (SOC) for 4.0 %, 2.0 %, and 1.0 % impurity concentrations.

Concentration	m_t (μ_B)	M (emu/g)	Co (μ_B)	W_{N1} (μ_B)	W_{N2} (μ_B)	W_{N3} (μ_B)	W_{N4} (μ_B)	Se_{N1} (μ_B)	Se_{N2} (μ_B)	Se_{N3} (μ_B)	Se_{N4} (μ_B)	E_g (eV)
4.0 %	2.98	1.98	2.26	-0.002	-0.002	0.009	-0.004	0.082	-0.004	0.003	0.000	0.06
2.0 %	2.98	1.67	2.27	0.000	-0.002	0.008	-0.002	0.081	-0.004	0.003	0.000	0.14
1.0 %	2.98	0.49	2.26	0.000	-0.002	0.008	-0.002	0.082	-0.004	0.003	0.000	0.14

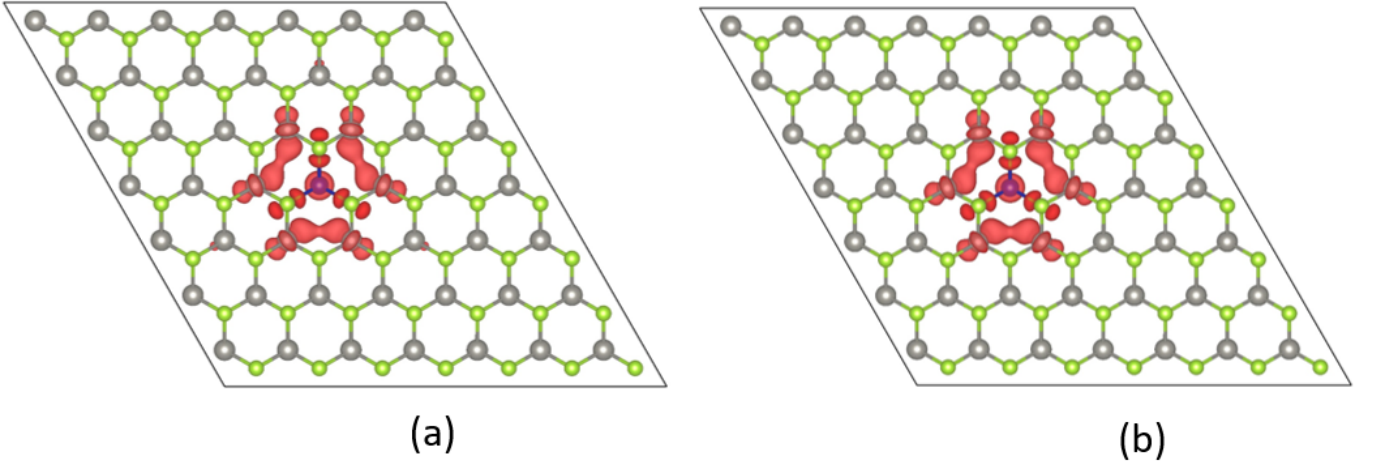


FIG. 10: 3D representation of iso-surface plot of band decomposed charge density for (a) valence band maximum (VBM) and (b) conduction band minimum (CBM) in $7 \times 7 \times 1$ (2.0 % impurity concentration) with isosurface value ranging from $\pm 6.7 \times 10^{-3} \mu_B/\text{\AA}^3$ for spin down in blue and spin up in red within the inclusion of SOC. The figure shows the VBM and CBM are contributed mainly by the spin up charges from the dopant atom Co, and the nearest W and Se atoms

the periodic boundary conditions (PBC) in the ab directions. All the internal coordinates including atom positions of these supercells were fully relaxed in each FM, and AFM configurations using the gamma centered k-mesh of $12 \times 12 \times 1$, $12 \times 6 \times 1$, $10 \times 5 \times 1$, $8 \times 4 \times 1$, $6 \times 3 \times 1$, $4 \times 2 \times 1$, $2 \times 1 \times 1$, and $1 \times 1 \times 1$ respectively. The ferromagnetic stability in the supercell is determined by the total energy difference between antiparallel (AFM) and parallel (FM) spins or the exchange coupling given by $\Delta E = E_{AFM} - E_{FM}$. If the difference is positive, the FM configuration is more stable and if the difference is negative, the AFM configuration is more stable. It has been predicted that the magnetic coupling in Co_W defect is very sensitive to the impurity concentration and the distance between the two dopant atoms. The magnetic coupling is AFM at high impurity concentration of 50.0 % and at the nearest neighbor separation of 3.43 Å for two Co atoms. The FM coupling persists until the Co-Co distance reaches 20.00 Å and the corresponding impurity concentration becomes 2.8 %. It becomes weakly AFM when the distance between the defects is as large as 23.30 Å and the impurity concentration becomes as low as 2.0 % as shown in Fig.11

To study the magnetic interaction with varying concentration at fixed spatial position of two Co atoms, we first calculated the formation energy at Se rich environment with two Co atoms doped in $4 \times 8 \times 1$ supercell at different possible configurations of Co-Co separation. The doped pair is denoted by $\text{Co}(0,i)$ where one Co atom occupies the fixed position at (0,0) and the other Co atom is substituted at the position of W atom marked with $i = 1-7$ within the supercell as shown in Fig.12(a). Here, we observed from the calculation of formation energy, that the two Co atoms tends to cluster at the nearest neighbor (NN) separation which is the equilibrium separation determined by the spatial positions (0,0) and (0,1) for the two Co atoms as shown in Fig.12(b). Then, the concentrations of the impurity atoms was varied to calculate the magnetic coupling with the two Co atoms at (0,0) and (0,1) in each supercell under consideration. When the two Co-atoms are fixed at their NN separation, the magnetic interaction depends uniquely on the impurity concentration. The FM coupling is strong when the impurity concentration varies from 11.1 % to as low as 1.6 % though there is slight reduction in ferromagnetism when the strength of defect goes on decreasing as shown in Fig.13. The curie temperature T_C is determined in ferromagnetic cases via mean field approximation (MFA) using Eqn.3 when the two Co atoms are at (0,0) and (0,1) positions in each supercell.

$$\frac{3}{2} K_B T_c = (E_{AFM} - E_{FM})/N \quad (3)$$

where $\Delta E = E_{AFM} - E_{FM}$, is the absolute value of exchange coupling, K_B is the Boltzmann constant, N is the number of Co dopants in the monolayer of WSe_2 . The curie temperature is determined to be 390 K, 403 K, 414 K, 590 K, and 990 K at impurity concentrations of 1.6 %, 2.0 %, 4.0 %, 6.2 %, and 11.1 % respectively. We predicted that the T_C is decreasing with decreasing magnetic impurity concentration satisfying the Zener model [59] which agrees with experimental reports. Our calculated value of T_C , greater than room temperature (300K), for 2.0 % and 1.0 % impurity concentration is overestimated with the experimental value [48]. The reason for overestimation is due to the spin waves (magnons) which are the magnetic analogues to the elastic lattice vibrations (phonons). So, T_C in MFA is given by the average value of magnon energies and these magnons are approximated with equal weight in

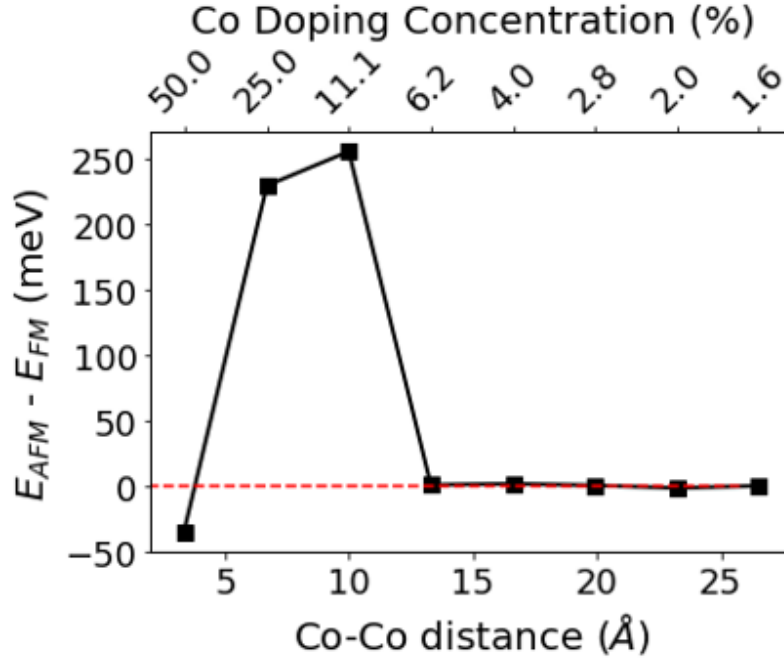


FIG. 11: AFM-FM configuration with simultaneous variation of Co-Co distance and Co Doping concentration.

MFA [60, 61].

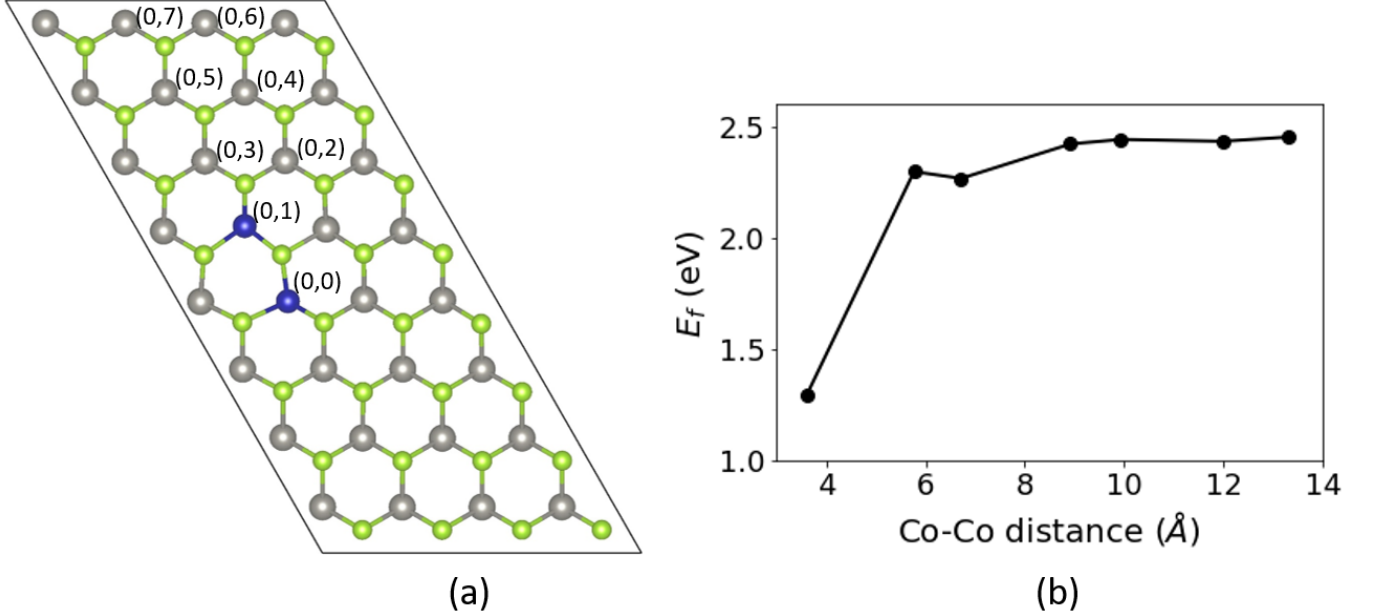


FIG. 12: (a) The spatial positions of two Co atoms doped in monolayer of $4 \times 8 \times 1$ supercell in which one Co atom is fixed at (0,0) position and the other at W position marked with (0,i), where $i = 1-7$, (b) calculation of formation energy for two Co atoms doped at varying distances given in Fig.(a).

Next, we studied the corresponding direction dependent magnetization from the in-plane (100) and out of plane (001) energy difference in terms of magnetic anisotropy energy (MAE) as given by eqn.4

$$MAE = E_{100} - E_{001} \quad (4)$$

where E_{100} , and E_{001} are the in-plane energy along x-axis (hard axis), and out of plane energy along z-axis (easy axis) respectively [62]. Here, MAE gives the energy required to deflect the magnetic moment in a crystal from the

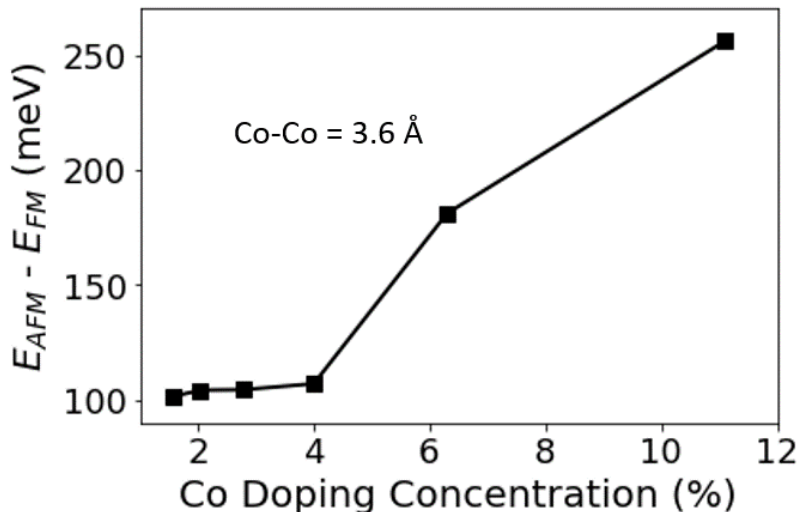


FIG. 13: AFM-FM configuration with respect to Co doping concentration with two Co atoms doped at NN separation of 3.6 Å

favorable (easy) direction to other spatial (hard) direction of the magnetization. Moreover, MAE is associated with the intrinsic properties of the materials which arises mainly due to the spin orbit coupling (SOC) interaction [63]. Thus, E_{100} and E_{001} energies have been determined by means of full relativistic self consistent energy calculations using the pre-converged charge and magnetization densities [64–66]. We observed the calculated energy E_{001} along z-axis was less than that of energy E_{100} along x-axis in all the concentrations indicating the preferential perpendicular magnetization along (001) plane. Therefore, Co atom introduces out of plane magnetic moment in the WSe₂ layers. Surprisingly, our results suggest that MAE is increasing with decreasing concentration and the value of MAE for 4.0 %, 2.0 %, and 1.0 % impurity concentrations are 38.5 meV, 55.2 meV, and 57.6 meV respectively. Our calculated value of MAE for 4.0 % Co-doping is analogous to that of Yu-Xi Song et al. obtained on Co_W defect on WS₂ monolayer [34].

IV. CONCLUSION

In conclusion, Co dopant in ML WSe₂ is energetically favorable to occupy the substitutional lattice site on W position under Se rich regime. The substitution of Co atom on the W atom imparts high magnetic moment of 3.00 μ_B and 2.98 μ_B per Co atom without using SOC and with using SOC respectively. The reason for the origination of such a high magnetic moment is due to the d orbitals of the Co and the nearest W atoms, and the p orbitals of the Se atoms via $d - p$ hybridization. Interestingly, we observed the significant dominating nature of the Hund's exchange splitting (ΔH_{ex}) over the crystal field splitting (Δ_{cf}) by 0.37 eV and 0.33 eV without SOC and with SOC respectively. However, the strength of the magnetization is strongly dependent on the doping concentration. Higher the doping concentration, higher the magnetization and vice-versa. The formation energy for the substitution of the two Co atoms reveal the fact that the two Co atoms tends to cluster at the nearest neighbor separation. It has been observed that the strength of ferromagnetism decays substantially with increasing Co-Co distance (decreasing Co concentration). However, it decays gradually when only impurity concentration is lowered and the two Co atoms are fixed at their NN separation. Thus, We reported a strong dependence of the magnetic interaction with the spatial positions, and concentrations of the dopant atoms. Moreover, the Curie temperature increases with increasing doping concentration based on the Zener model. The promising high value of MAE suggests the applications of this defect material in magnetic storage devices besides spintronics and optoelectronics.

V. CONFLICT OF INTEREST

The authors declare no conflict of interest.

VI. ACKNOWLEDGEMENTS

This work was supported by a National Research Foundation of Korea (NRF) grant funded by the Korean government (Ministry of Science, ICT & Future Planning) (No.2015M3D1A1070639) and in part by the Center for Computational Sciences (CCS) at Mississippi State University.

-
- [1] A. K. Geim and K. S. Novoselov, in *Nanoscience and Technology: A Collection of Reviews from Nature Journals* (World Scientific, 2010) pp. 11–19.
- [2] Y. Gong, Z. Liu, A. R. Lupini, G. Shi, J. Lin, S. Najmaei, Z. Lin, A. L. Elías, A. Berkdemir, G. You, *et al.*, *Nano letters* **14**, 442 (2014).
- [3] H. L. Zhuang and R. G. Hennig, *Chemistry of Materials* **25**, 3232 (2013).
- [4] R. Suzuki, M. Sakano, Y. Zhang, R. Akashi, D. Morikawa, A. Harasawa, K. Yaji, K. Kuroda, K. Miyamoto, T. Okuda, *et al.*, *Nature nanotechnology* **9**, 611 (2014).
- [5] D. H. Keum, S. Cho, J. H. Kim, D.-H. Choe, H.-J. Sung, M. Kan, H. Kang, J.-Y. Hwang, S. W. Kim, H. Yang, *et al.*, *Nature Physics* **11**, 482 (2015).
- [6] H. J. Conley, B. Wang, J. I. Ziegler, R. F. Haglund Jr, S. T. Pantelides, and K. I. Bolotin, *Nano letters* **13**, 3626 (2013).
- [7] A. McCreary, R. Ghosh, M. Amani, J. Wang, K.-A. N. Duerloo, A. Sharma, K. Jarvis, E. J. Reed, A. M. Dongare, S. K. Banerjee, *et al.*, *ACS nano* **10**, 3186 (2016).
- [8] A. M. Jones, H. Yu, N. J. Ghimire, S. Wu, G. Aivazian, J. S. Ross, B. Zhao, J. Yan, D. G. Mandrus, D. Xiao, *et al.*, *Nature nanotechnology* **8**, 634 (2013).
- [9] Y. Nakamura and Y. Yanase, *Physical Review B* **96**, 054501 (2017).
- [10] X. Liu, Z. Zhang, C. Cai, S. Tian, S. Kushwaha, H. Lu, T. Taniguchi, K. Watanabe, R. J. Cava, S. Jia, *et al.*, *2D Materials* **4**, 021018 (2017).
- [11] P. Hankare, A. Manikshete, D. Sathe, P. Chate, A. Patil, and K. Garadkar, *Journal of alloys and compounds* **479**, 657 (2009).
- [12] E. Gourmelon, O. Lignier, H. Hadouda, G. Couturier, J. Bernède, J. Tedd, J. Pouzet, and J. Salardenne, *Solar energy materials and solar cells* **46**, 115 (1997).
- [13] B. Radisavljevic, A. Radenovic, J. Brivio, V. Giacometti, and A. Kis, *Nature nanotechnology* **6**, 147 (2011).
- [14] A. M. Seayad and D. M. Antonelli, *Advanced Materials* **16**, 765 (2004).
- [15] K. Chang and W. Chen, *ACS nano* **5**, 4720 (2011).
- [16] A. C. Hewson and J. Kondo, *Scholarpedia* **4**, 7529 (2009).
- [17] E. Marseglia, *International reviews in physical chemistry* **3**, 177 (1983).
- [18] J. A. Wilson and A. Yoffe, *Advances in Physics* **18**, 193 (1969).
- [19] A. Dias, F. Qu, D. L. Azevedo, and J. Fu, *Physical Review B* **98**, 075202 (2018).
- [20] Y. Cheng, Z. Zhu, W. Mi, Z. Guo, and U. Schwingenschlögl, *Physical Review B* **87**, 100401 (2013).
- [21] K. Sato, L. Bergqvist, J. Kudrnovský, P. H. Dederichs, O. Eriksson, I. Turek, B. Sanyal, G. Bouzerar, H. Katayama-Yoshida, V. Dinh, *et al.*, *Reviews of modern physics* **82**, 1633 (2010).
- [22] L. Seixas, A. Carvalho, and A. C. Neto, *Physical Review B* **91**, 155138 (2015).
- [23] I. Žutić, J. Fabian, and S. D. Sarma, *Reviews of modern physics* **76**, 323 (2004).
- [24] R. Mishra, W. Zhou, S. J. Pennycook, S. T. Pantelides, and J.-C. Idrobo, *Physical Review B* **88**, 144409 (2013).
- [25] X. Zhao, C. Xia, X. Dai, T. Wang, P. Chen, and L. Tian, *Journal of Magnetism and Magnetic Materials* **414**, 45 (2016).
- [26] B. Li, T. Xing, M. Zhong, L. Huang, N. Lei, J. Zhang, J. Li, and Z. Wei, *Nature communications* **8**, 1 (2017).
- [27] S. Mekonnen Hailemariam, *Advances in Condensed Matter Physics* **2020** (2020).
- [28] W. Yu, Z. Zhu, C.-Y. Niu, C. Li, J.-H. Cho, and Y. Jia, *Nanoscale research letters* **11**, 1 (2016).
- [29] A. Mitioglu, P. Plochocka, Á. Granados del Aguila, P. Christianen, G. Deligeorgis, S. Anghel, L. Kulyuk, and D. Maude, *Nano letters* **15**, 4387 (2015).
- [30] J. Coey, *IEEE Transactions on magnetics* **47**, 4671 (2011).
- [31] G. Kresse and D. Joubert, *Physical review b* **59**, 1758 (1999).
- [32] G. Kresse and J. Furthmüller, *Phys. Rev. B* **54**, 11169 (1996).
- [33] G. Kresse and J. Furthmüller, *Computational materials science* **6**, 15 (1996).
- [34] Y.-X. Song, W.-Y. Tong, Y.-H. Shen, S.-J. Gong, Z. Tang, and C.-G. Duan, *Journal of Physics: Condensed Matter* **29**, 475803 (2017).
- [35] D. Thapa, V. Dixit, S. KC, B. Lamichhane, C. N. Nandadasa, J. Song, K. Lee, S. W. Kim, and S.-G. Kim, *arXiv preprint arXiv:2106.10757* (2021).
- [36] S. Y. Lee, J. Bang, H. Y. Song, B. I. Yoo, Y. Kim, K. Lee, D. Thapa, S.-G. Kim, and S. W. Kim, *npj Quantum Materials* **6**, 1 (2021).
- [37] S. Dudarev, G. Botton, S. Savrasov, C. Humphreys, and A. Sutton, *Physical Review B* **57**, 1505 (1998).
- [38] L. Wang, T. Maxisch, and G. Ceder, *Physical Review B* **73**, 195107 (2006).
- [39] Y.-L. Lee, J. Kleis, J. Rossmeisl, and D. Morgan, *Physical Review B* **80**, 224101 (2009).
- [40] S. Selcuk and A. Selloni, *The Journal of Physical Chemistry C* **119**, 9973 (2015).
- [41] H. Ding, A. V. Virkar, M. Liu, and F. Liu, *Physical Chemistry Chemical Physics* **15**, 489 (2013).

- [42] C. Zhang and P. Bristowe, RSC advances **3**, 12267 (2013).
- [43] M. Bajdich, M. García-Mota, A. Vojvodic, J. K. Nørskov, and A. T. Bell, Journal of the American chemical Society **135**, 13521 (2013).
- [44] M. García-Mota, M. Bajdich, V. Viswanathan, A. Vojvodic, A. T. Bell, and J. K. Nørskov, The Journal of Physical Chemistry C **116**, 21077 (2012).
- [45] M. Higashiwaki, K. Sasaki, A. Kuramata, T. Masui, and S. Yamakoshi, Applied Physics Letters **100**, 013504 (2012).
- [46] K. Momma and F. Izumi, Journal of applied crystallography **44**, 1272 (2011).
- [47] U. Herath, P. Tavazde, X. He, E. Bousquet, S. Singh, F. Muñoz, and A. H. Romero, Computer Physics Communications, 107080 (2019).
- [48] S. Ahmed, X. Ding, P. P. Murmu, N. N. Bao, R. Liu, J. Kennedy, J. Ding, and J. Yi, Journal of Alloys and Compounds **731**, 25 (2018).
- [49] B. W. Baugher, H. O. Churchill, Y. Yang, and P. Jarillo-Herrero, Nature nanotechnology **9**, 262 (2014).
- [50] S. Kumar and U. Schwingenschlogl, Chemistry of Materials **27**, 1278 (2015).
- [51] P. V. Medeiros, S. Stafström, and J. Björk, Physical Review B **89**, 041407 (2014).
- [52] P. V. Medeiros, S. S. Tsirkin, S. Stafström, and J. Björk, Physical Review B **91**, 041116 (2015).
- [53] D. Thapa, *Tunable electronic and magnetic properties in 2D-WSe₂ monolayer via vanadium (V) doping and chalcogenide (Se) vacancies: A first-principle investigations*, Ph.D. thesis, Mississippi State University (2021).
- [54] N. Wu, X. Zhao, and T. Wang, Physica E: Low-dimensional Systems and Nanostructures **84**, 505 (2016).
- [55] T. Onishi, in *Advances in Quantum Chemistry*, Vol. 64 (Elsevier, 2012) pp. 31–81.
- [56] B. Huang, H. Xiang, J. Yu, and S.-H. Wei, Physical review letters **108**, 206802 (2012).
- [57] C. J. Gil, A. Pham, A. Yu, and S. Li, Journal of Physics: Condensed Matter **26**, 306004 (2014).
- [58] D. L. Duong, S. J. Yun, Y. Kim, S.-G. Kim, and Y. H. Lee, Applied Physics Letters **115**, 242406 (2019).
- [59] S. J. Yun, D. L. Duong, M.-H. Doan, K. Singh, T. L. Phan, W. Choi, Y.-M. Kim, and Y. H. Lee, arXiv preprint arXiv:1806.06479 (2018).
- [60] R. Skomski and J. Coey, *Permanent magnetism* (Routledge, 2019).
- [61] S. Li, Z. Ao, J. Zhu, J. Ren, J. Yi, G. Wang, and W. Liu, The journal of physical chemistry letters **8**, 1484 (2017).
- [62] V. Dixit, D. Thapa, B. Lamichhane, C. N. Nandadasa, Y.-K. Hong, and S.-G. Kim, Journal of Applied Physics **125**, 173901 (2019).
- [63] J. H. van Vleck, Physical Review **52**, 1178 (1937).
- [64] X. Wang, D.-s. Wang, R. Wu, and A. J. Freeman, Journal of magnetism and magnetic materials **159**, 337 (1996).
- [65] D. Li, A. Smogunov, C. Barreateau, F. Ducastelle, and D. Spanjaard, Physical Review B **88**, 214413 (2013).
- [66] D. J. Sellmyer and R. Skomski, *Advanced magnetic nanostructures* (Springer Science & Business Media, 2006).